



Trade Science Inc.

Research & Reviews In

Electrochemistry

Full Paper

RREC, 4(2), 2013 [48-60]

Multiwalled carbon nanotubes incorporated quaternized polysulfone composites for alkaline membrane fuel cells

Rajangam Vinodh, Dharmalingam Sangeetha*

Department of Chemistry, Anna University, Chennai – 600025, Tamil Nadu, (INDIA)

E-mail : sangeetha@annauniv.edu

ABSTRACT

A novel quaternized polysulfone/functionalized MWCNT (QPSU/*f*-MWCNT) composite polymer membrane was prepared, using the solution casting method. The characteristic properties of the QPSU/MWCNT composite membranes were investigated, using the FTIR, UV-Visible spectroscopy, thermo gravimetric analysis (TGA), scanning electron microscopy (SEM), X-ray diffraction (XRD) and Raman spectroscopy. Alkaline membrane fuel cell (AMFC) comprised QPSU/*f*-MWCNT composite membrane, were prepared and examined. The experimental results reveal that the AMFC employing a cheap non-perfluorinated (QPSU/*f*-MWCNT) composite membrane which shows excellent electrochemical performances. The maximum H₂/O₂ fuel cell performance was achieved for QPSU/5% *f*-MWCNT membrane with a power density of 190 mW cm⁻². The composite membranes were subjected to cyclic voltammetry studies for methanol oxidation. The direct methanol alkaline membrane fuel cell (DMAMFC), exhibits a maximum power density of 65 mW cm⁻² for QPSU/5% *f*-MWCNT membrane. © 2013 Trade Science Inc. - INDIA

KEYWORDS

Multiwalled carbon nanotubes;
Quaternized polysulfone;
Anion exchange membrane;
Cyclic voltammetry;
Fuel cell.

INTRODUCTION

Fuel cell systems hold promise as alternative power sources for a range of applications from automobiles to portable electronic appliances, due to their high efficiency, high energy density, and low emissions^[1]. For low temperature fuel cells, polymer electrolyte membrane based fuel cells (PEMFCs) are considered most promising^[2]. The widespread market penetration of these PEMFCs has yet to be realized mainly due to their high costs (platinum (Pt) catalysts, Nafion membranes), insufficient durability, and system limitations^[3].

The most important advantage of alkaline fuel cells (AFCs) over their acidic counterparts is their greatly improved oxygen reduction kinetics as well as a better fuel oxidation kinetics^[4-7]. These improvements can lead to higher efficiencies and enable the use of non noble metal catalysts, greatly reducing the cost of the device. Indeed, hydrogen fueled AFCs can outperform all known low temperature fuel cells^[5]. However, AFCs have traditionally employed liquid alkaline electrolytes containing metal hydroxides (e.g., potassium hydroxide) that react with CO₂ to form metal bicarbonates, and subsequently carbonate salts. If sufficiently high levels

of these salts are formed, they can precipitate out of the solution, decreasing the electrolyte conductivity and eventually obstructing the electrode pores, of which reduce power output^[8,9]. Polymers with anchored organic cations hold great promise as alkaline anion exchange membranes (AEMs), because their cations cannot aggregate with anions to form a crystal lattice. Therefore this enables operation under alkaline conditions in the presence of CO₂^[5,10]. Additionally, in an alkaline membrane fuel cell (AMFC) or direct methanol alkaline membrane fuel cell (DMAMFC), the direction of the hydroxide ion conduction opposes methanol crossover, thereby mitigating or possibly eliminating this process^[5,11]. Although AEMFCs offer important potential advantages, the lower ionic conductivity of AEMs compared to Nafion[®] is of great concern, because it may lower the performance. Significant research effort has been focused on the development of new AEMs for AMFC and DMAMFC, but so far only a few AEMs have been evaluated for alkaline fuel cell applications^[5,12-17].

In this report, we chose polysulfone as a starting material to synthesize the alkaline anion exchange membrane. The synthetic protocol for the quaternized polysulfone (QPSU) based AEMs have been described in our earlier report^[18]. However, the main issue with the anion exchange membrane is its low stability under the working conditions of the AMFC (i.e. 60 °C and high pH) due to S_N2 substitution and Hofmann elimination^[19]. To overcome these limitations, carbon nanotubes were incorporated into the AEM, which was expected to improve the thermal and mechanical stabilities.

It would be more advantageous to investigate new combinations of the existing materials as hybrid materials, blends, and nanocomposites for utilization of their complementary properties^[20,21]. In this context, there is a renewed interest in developing quaternized polymer/CNT composites as novel futuristic materials. One of the main reasons is due to its common applications of the two components which offer the possibility to observe its synergistic effects. Carbon nanotubes (CNTs), which consist of single or a number of graphene layers, have fascinated much attention as a reinforcing material for polymers, due to their excellent mechanical properties, low density and high aspect ratio^[22,23]. Recent research results on CNT-reinforced polymer composites

have revealed that physical properties, such as tensile modulus and strength, are affected by the amount of nanotubes and their state of dispersion (or alignment) within the polymer matrices^[23]. Secondary force interactions and stress/deformations arise from mismatching coefficients of the thermal expansion between CNTs and polymers were recommended as the governing factors for CNT-polymer matrix adhesion. To date, however, despite the abovementioned advantageous properties, CNT-incorporated composite membranes have not been well exploited for fuel cell applications^[24].

To the reports pertaining, the fabrication of a composite membrane using MWCNT as a filler material and quaternized polysulfone as a polymer electrolyte membrane towards solid alkaline membrane fuel cell, has not been reported elsewhere. The present article describes the preliminary work in detail, the successful synthesis of a composite membrane by the solution casting technique, which exhibits significant thermal and chemical stability with no loss of conductivity. This constitutes a breakthrough that allows the successful application of this form of composite membranes in fuel cells. The composite membrane (QPSU/*f*-MWCNT) produced was characterized, using FTIR, UV-Visible and Raman spectroscopy. Ex situ physical characterizations included TGA, XRD, tensile strength and SEM analyses and measurement of the ionic conductivity, ion exchange capacity and methanol permeability. The most important objective was to evaluate the composite membrane performance in a real scale AMFC and DMAMFC. The composite membranes were tested with their cell voltage and power density values in a 25 cm² electrode cell area.

EXPERIMENTAL

Materials

Polysulfone (PSU, 500g) (CAS No. 25154-01-2) was purchased from Sigma-Aldrich (USA). A multiwalled carbon nanotube (MWCNT, 10-15 nm) (CAS No. 25154-01-2) was purchased from Sigma Aldrich (USA) with a purity of 99%. Other chemicals like dimethylformamide (DMF), conc. nitric acid and sulphuric acid were purchased from E-Merck (India). All were of an analytical grade, and were used as received.

Full Paper

20% of Pt on Vulcan XC-72 purchased from Arora-Mathey Pvt. Ltd., India, was used as an anode catalyst. Polytetrafluoroethylene (PTFE) binder (CAS No. 9002-84-0), 60 wt % dispersion in water and IPA were purchased from Sigma-Aldrich (USA). Carbon cloth was obtained from Cabot carbon Inc., Germany. 10% Ag on Vulcan XC-72 was synthesized in our lab^[25] and was used as a cathode catalyst. For the DMAMFC, Pt/C and Pt-Ru/C were used as the anode and cathode materials that were purchased from Arora-Mathey Pvt. Ltd., India. All the solutions were prepared with double distilled water.

Functionalization of the MWCNTs

The as-received MWCNTs (1g) were first treated with 50 mL of 3:1 mixture of concentrated sulfuric and nitric acid, and ultra sonicated for 16 h to introduce carboxylic acid groups on the MWCNT surface. Upon completion, the mixture was subjected to repeated cycles of washing with cold distilled water, to remove the residual acid followed by centrifugation until the supernatant of the mixture attained the pH 7, which indicated nil acidity in the suspension. The sample was then dried in a vacuum oven at 100 °C for 6 h.

Preparation of the composite membrane

QPSU/*f*-MWCNT composite membranes were prepared by casting a solution of the alkaline form of QPSU and *f*-MWCNT. QPSU was first dissolved in DMF at room temperature and then *f*-MWCNT was added slowly over time with constant stirring. The percentage of *f*-MWCNT in the mixture was varied from 2.5 to 5%. The stirring was continued for another 24 h. The solution was then subjected to ultra sonication for 15 minutes. The resultant viscous fluid mixture was then spread on a glass plate with the help of a doctor's knife. The film was dried at 70 °C for 8 h and then at 50 °C for 6 h.

Fourier transform infra red (FTIR)

The interaction of the polymer with multi walled carbon nanotubes was determined by FTIR. The FTIR spectra of QPSU and their corresponding composite membranes were recorded in the transmission mode, using the Perkin Elmer spectrometer by placing the membranes in KBr window.

Water absorption

The water content (W_c) of the final membrane was determined, after equilibrating a sample of the membrane in deionized water at room temperature. The membrane samples were removed from the water and weighed immediately after blotting the free surface water. Then, it is dried for over 4 h at 80 ± 5 °C. The water content was deduced from the difference in weight between the wet (W_1) and the dry (W_2) membrane in unit gram H_2O/g dry membrane based on the following formula^[26],

$$W_c (\%) = (W_1 - W_2) / W_2 \times 100$$

Ion exchange capacity

The ion exchange capacity (IEC) of the membrane was determined, the following procedures described elsewhere^[27]. The quaternized polymer membrane was soaked in 1 M potassium hydroxide (alkali) solution for 24 h to convert the Cl form into the OH form. Then, the membrane was washed and soaked in deionized water for 24 h to remove the attached alkali. The membrane was then equilibrated with 50 ml of 0.01M HCl aqueous solution for 24 h, followed by back titration for the determination of the IEC.

Ionic conductivity

The ion conductivity of the membrane was evaluated, by using the AC impedance analyzer with an amplitude of 20 mV and a frequency range of 1 Hz – 500 kHz. Each membrane was fitted in a Teflon conductivity test cell that consisted of two Pt wires (a counter electrode and a working electrode) and two Pt foils (reference electrode 1 and reference electrode 2). Membrane resistance was calculated using the intercept value of the real axis (Z') in the complex plane, which is composed of the real axis and the imaginary axis (Z''). Ionic conductivity was calculated via the following equation,

$$\text{Conductivity (S/cm)} = \frac{L}{(R \times A)}$$

Where,

R= Sample resistance, Ω , L= Wet sample thickness, cm and A= Sample area, cm^2

Methanol permeability and selectivity ratio

Methanol permeability measurements^[28,29] were

taken using a diffusion cell. The cell was divided into two compartments; one was filled with deionized water (called B compartment), and the other compartment filled with a 20 wt % methanol aqueous solution (called A compartment). Prior to testing, the prepared membranes were hydrated in deionized water for at least 24 hours. The membrane with a surface area of 0.58 cm² was sandwiched by an O-ring and clamped tightly between two compartments. The magnetic stir bar was kept dynamic in the glass diffusion cell during the experiment. The concentration of methanol diffused from compartment A to B across the membrane was examined, using a digital refractometer. An aliquot of 0.20 mL was sampled from the B compartment every 30 minutes. Before the permeation experiment, a calibration curve for the value of density vs. the methanol concentration was prepared. The calibration curve was used to calculate the methanol concentration in the permeation experiment. The methanol permeability was calculated from the slope of the straight-line plot of methanol concentration vs. permeation time. The methanol concentration in the B compartment as a function of time, is given in the equation below,

$$C_B(t) = (A/V)(DK/L)C_A(t-t_0)$$

Where, C is the methanol concentration (mol L⁻¹), A and L are the polymer membrane area (cm²) and thickness (μm), D and K is the methanol diffusivity and partition coefficient between the membrane and the solution. The product DK is the membrane permeability (P), t₀, a time lag, is related to the diffusivity (D): t₀ = L²/6D.

An electrolyte membrane, particularly DMAMFC, should have two important properties; one is its ionic conductivity should be the maximum and the other one is the methanol diffusion should be the minimum. Hence, the higher the ratio of ionic conductivity to methanol permeability (referred to as the selectivity ratio), the better would be the membrane performance in the DMAMFC. This selectivity ratio is an indication of the performance of the electrolyte membrane.

Hydrolytic and alkaline stability test

The boiling water test (hydrolytic stability test) was carried out by immersing the membrane in water and heating the water to its boiling point, whereas in the alkaline stability test, the membrane was immersed in a

5 M sodium hydroxide solution over a period of time.

Alkaline stability test (or durability test) was carried out to examine the durability of the membrane in the fuel cell condition. In general, the polymer membrane, which undergoes degradation when fuel cell is operated, can be found out using this method.

UV-visible spectroscopy

UV-Vis analysis was monitored on a T 90+ (PG Instruments) UV-Visible spectrometer, in the wavelength range of 200–800 nm with a scanning speed of 200 nm/min.

Thermogravimetric analysis (TGA)

A TGA analyzer (TGA model Q50 V20.6 build 31 systems) was used to test the thermal stability of the QPSU and its composite membranes. QPUS and its composite membranes were heated from room temperature to 800 °C at a heating rate of 10 °C min⁻¹ under nitrogen atmosphere.

Scanning electron microscopy (SEM)

A scanning electron microscopy was used to view the surface of the polymer membrane and also to predict the distribution of the nano particles into the polymer matrix, and the size of the particles. The SEM micrographs were obtained with the help of HITACHI S-3400 equipped with an energy dispersive X-ray analyzer. The QPSU and QPSU/5% f-MWCNT composite membranes were dried and then coated with gold to view the SEM images.

Mechanical properties

The mechanical property of the membranes can be determined using Universal Testing Machine (UTM). The tensile testing was done according to ASTM D 638 standard. Hounsfield UTM was used for this purpose with a cross head speed of 2 mm/min and maximum load of 5000 N. The samples were cut into pieces of 5 mm x 50 mm (Thickness of the membrane 85 ± 5 μm). For each testing at least three measurements were taken and the average value was reported.

X-ray diffraction (XRD)

The membrane sample was subjected to X-ray diffraction studies with Rich Seifert X-ray diffractometer, using CuKα radiation of wavelength 1.5418 Å with a

Full Paper

scan speed of 0.2°/sec. The peaks observed from the X-ray diffraction spectrum were analyzed and indexed, using the Proszki software package.

Raman spectroscopy

Raman spectrum is a simple tool to characterize the QPSU/*f*-MWCNT composite polymer membrane. Raman spectroscopy analysis was carried out using Raman R3000 System, and by using a 509 working-length objective (8 mm). Raman excitation source was provided by 532 nm He–Ar laser beam with a beam power of 0–90 mW and was focused on the sample with a spot size of about 1 μm in diameter.

Cyclic voltammetry studies

Cyclic voltammetry studies were performed using a three electrode system, equipped with CH electrochemical working station at a temperature of 293±5 K. All the experimental solutions were prepared in double distilled water and were thoroughly degassed with nitrogen throughout the experiments. The glassy carbon electrode (GCE) served as the working electrode with an area of 0.0707 cm². Pt wire and saturated calomel electrode (SCE) were used as the counter and reference electrodes, respectively. All potentials given in this study were with respect to the SCE reference electrode. The potential range was scanned from -1.0 to 1.0 V with the scan rate of 50 mVs⁻¹.

(a) Fabrication of the working electrode

The GCE was polished to a mirror finish with 0.1 μm alumina powder before each experiment and served as principal substrate of the working electrode. In order to prepare the modified electrode (i.e. QPSU/GCE), the QPSU ionomer was well dispersed ultrasonically in cyclohexane at a concentration of 1 mg/mL, and 15 μL of the aliquot was transferred on to a polished glassy carbon disc electrode. After volatilization of the solvent, the resultant modified electrode was used as the working electrode. The same procedure was adopted for the QPSU/*f*-MWCNTs composites too.

Fabrication of the MEA and AMFC performance study

The membrane electrode assembly (MEA) structure is poised of an electrolyte membrane coated by a catalyst on both the anode and cathode sides, and sand-

wiched by a gas diffusion layer. The preparation of the diffusion layer was discussed in our earlier report^[30]. After the preparation of the diffusion layer, the catalyst slurry ink was prepared with the help of carbon supported platinum black and silver catalyst with a loading of 0.5 mg cm⁻² and 0.375 mg cm⁻² respectively for the anode and cathode. Then, appropriate amount of distilled water and alcohol were mixed well using an ultra sonicator. After the ultra sonication, the black slurry was coated on to the respective diffusion layers. The as-prepared anode and cathode were dried in a vacuum oven at 100 °C for 2 hours, and then in a muffle furnace at 350 °C for six hours. The prepared virgin and its composite membranes were sandwiched between the prepared anode and cathode electrodes, and hot pressed at 80 °C with 1.5 ton pressure for about 2 minutes^[30].

The fuel cell tests were carried out using an indigenous fuel cell work station. A MEA, of an area of 25 cm², was protected between the two graphite plates, which had machined triple serpentine flow channels (1 mm channel width, 1 mm channel height and 1.5 mm rib width) and gold coated aluminum current collector plates. The fixture was preserved at a constant torque of 5.5 N m, using torque wrench and bolts. Fuel cell measurements were taken at 60 °C with H₂ and O₂ gases with flowing at the rate of 20 and 40 mL min⁻¹ respectively.

DMAMFC performance study

The above mentioned procedure remains the same for the direct methanol alkaline membrane fuel cell (DMAMFC). The only difference is the replacement of Pt/C by Pt-Ru/C as an anode catalyst for the DMAMFC; i.e., catalyst slurry ink was prepared with the help of carbon supported platinum-ruthenium black (Pt-Ru/C), and Pt/C catalyst with a loading of 0.5 mg cm⁻² and 0.375 mg cm⁻² respectively for the anode and cathode. Fuel cell measurements were taken at 60 °C with CH₃OH and O₂ gases with the flow rates of 20 and 40 mL min⁻¹ respectively.

RESULTS AND DISCUSSION

Functionalization of the MWCNT

There are two serious issues related with CNTs,

when these materials are used as reinforcements in polymer composites^[31]. A main problem is the aggregation of CNTs into bundles, resulting in weak interfacial bonding between the CNTs and the polymer matrix which leads to a decrease in the electrical and mechanical properties of the composites^[32]. To overcome this difficulty, it is essential to develop a strong interface between the fillers and the polymer. Then, the effectiveness of the load transfer could be improved. A commonly accepted approach towards this objective reported thus far in the literature is the surface functionalization of CNTs^[33,34]. Generally, covalent functionalization will make defects on the CNT surface, disrupting the extent of conjugation, and harmfully impacting the charge carrier mobility in CNTs^[35]. However, since MWCNTs are less prone to bundle than SWCNTs, and for the reason that it is possible to functionalize the surface layers only, the conductivity will not be reduced significantly^[36].

Carbon nanotubes functionalized with carboxylic acid groups were confirmed by the FTIR. Figure 1 represents the FTIR spectra of the MWCNT and functionalized MWCNT (*f*-MWCNT). There are four distinct absorption peaks at 1564, 2862, 2932 and 3440 cm^{-1} respectively in Figure 1 (b). The spectrum shows a band around 3440 cm^{-1} , which can be attributed to the hydroxyl group (-OH). Bands around 2932 and 2850 cm^{-1} were due to asymmetric and symmetric C-H stretching. In the acid-functionalized MWCNTs spectrum, the peak near 1560 cm^{-1} corresponds to the infrared-active phonon mode of the nanotubes, and the peaks at 1740 and 1250 cm^{-1} apparently correspond to the stretching mode of the carboxylic acid groups. These observations are clear indications of -COOH groups on the surface of the nanotubes.

Figure 2 represents the FE-SEM photographs of the as-purchased MWCNT and *f*-MWCNT, with their corresponding EDAX spectra. Pristine MWCNTs which have smooth surfaces, appeared as large bundles with lengths in the order of microns and diameters around 10–20 nm. After acid treatment, the *f*-MWCNTs were disentangled and roughed, and their lengths were slightly reduced by both the oxidation and ultrasonic treatment. The same was confirmed through the corresponding EDAX spectrum in the presence of other elements.

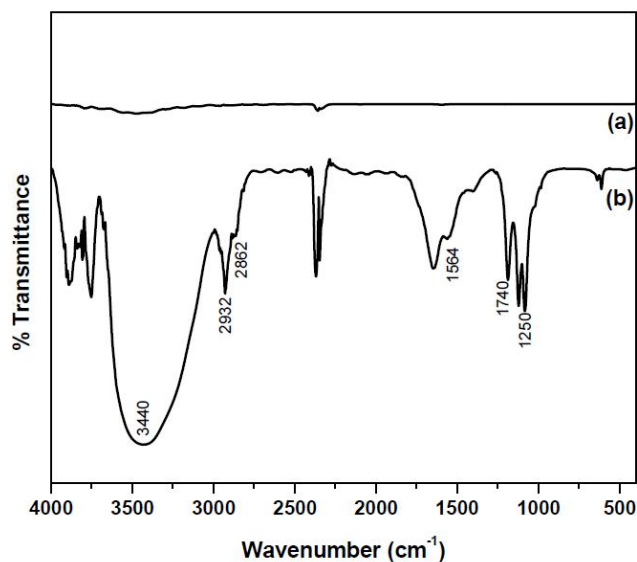


Figure 1: FTIR spectra of (a) MWCNT and (b) functionalized MWCNT.

Water absorption, ion exchange capacity and conductivity

Water uptake is an important parameter in studying the AMFCs, because the water that resides in the hydrophilic domains facilitates the transport of the OH⁻ ions. However, a large excess amount of water uptake will result in the loss of mechanical stability. The water absorption, IEC and conductivity values of the QPSU and their composite membranes are shown in TABLE 1. As expected, the water uptake values increased with an increase in the weight fraction of the *f*-MWCNT in the membrane. This increase in water absorption is due to the incorporation of the functionalized (-COOH) MWCNTs.

TABLE 1: Water absorption, IEC and conductivity values of QPSU/*f*-MWCNT composite membranes.

Membrane	Water absorption, %	IEC, meq/g	Conductivity, S/cm
QPSU	5.5	0.693	0.73×10^{-2}
QPSU/2.5% MWCNT	8.4	0.704	0.79×10^{-2}
QPSU/5% MWCNT	11.5	0.792	0.84×10^{-2}

The IEC indicates the intensity of exchangeable hydrophilic groups grafted onto the membrane matrix, which is responsible for their charged nature. The IEC of the composites also increased with an increase in the weight fraction of the *f*-MWCNT and the maximum IEC was found to be 0.792 meq/g for the QPSU/5% *f*-MWCNT.

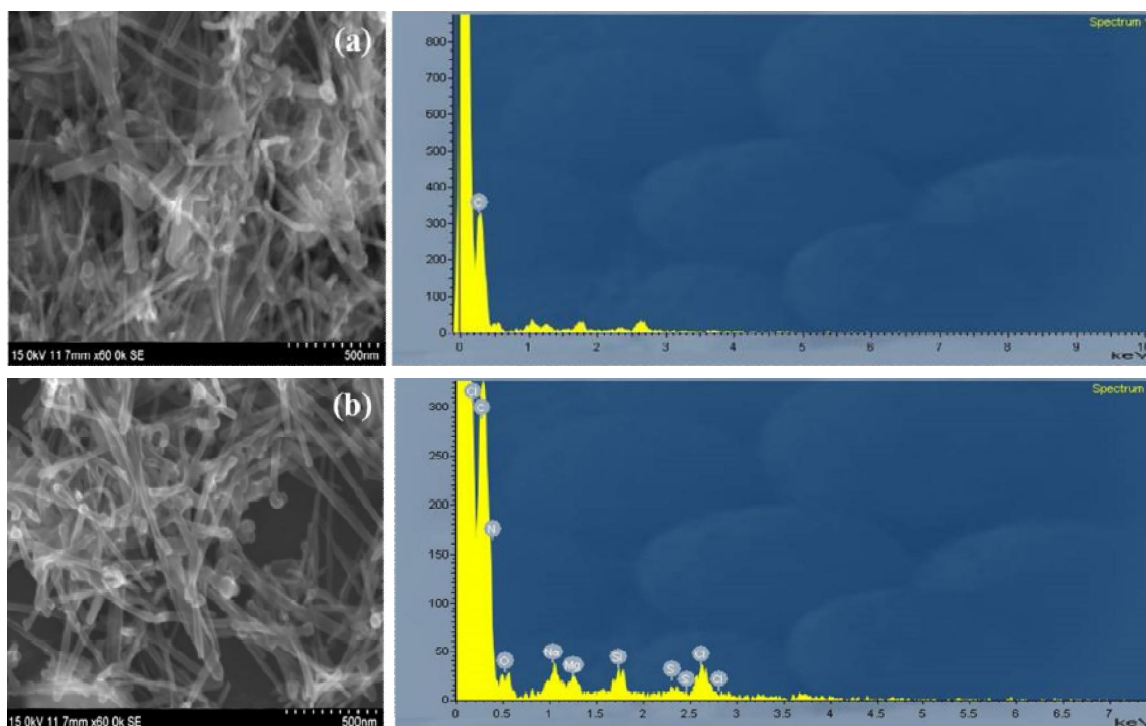


Figure 2 : FE-SEM images of (a) MWCNT, (b) *f*-MWCNT and their corresponding EDAX spectra.

One of the most important parameters that govern the suitability of a polymer electrolyte membrane for use in a fuel cell is its ionic conductivity. The ionic conductivity of pristine QPSU was found to be 0.73×10^{-2} S/cm. In the case of the composites, there is an increase in the ionic conductivity with an increase in the content of the *f*-MWCNT. This increasing trend might be attributed to the transportation of hydroxyl ions, which was facilitated by the presence of water molecules by the hopping mechanism. The increasing trend in ionic conductivity was also associated with the acidic site of *f*-MWCNT in the presence of water.

Methanol permeability and selectivity ratio

TABLE 2 shows the methanol permeability and selectivity ratio of the QPSU and *f*-MWCNT composite membranes. When compared with the QPSU, the permeation of methanol in the case of composites, i.e. *f*-MWCNT incorporated polymer matrix, there is a remarkable decrement in the methanol permeability. Also, the methanol permeability of QPSU/*f*-MWCNT is rather low when compared to the Nafion membrane. This is owing to the movement of the OH⁻ anions from the cathode to the anode, opposing the direction of the methanol flux. The methanol electro-osmotic effect depresses the methanol crossover through the membrane. The pristine QPSU

electrolyte membranes exhibited a selectivity ratio of 0.76×10^4 Ss/cm³, while the composite membranes exhibited higher selectivity ratio values than those of the pristine QPSU. It clearly revealed that the QPSU/*f*-MWCNT composite membranes can be successfully used in the DMAMFCs.

TABLE 2 : Methanol permeability and selectivity ratio of QPSU/*f*-MWCNT composite membranes.

Membrane	Methanol permeability, cm ² /s	Selectivity ratio, Ss/cm ³
QPSU	2.63×10^{-6}	0.28×10^4
QPSU/2.5% MWCNT	2.54×10^{-6}	0.31×10^4
QPSU/5% MWCNT	2.46×10^{-6}	0.34×10^4

Hydrolytic and alkaline stability

The property of IEC was measured after the hydrolytic and alkaline stability tests. The loss of IEC was found to be 1.14 to 1.73% for all the prepared membranes, which clearly revealed that the IEC was not significantly changed. This implies that the prepared QPSU/*f*-MWCNT composite membranes have good mechanical and chemical stability.

FTIR

The FTIR spectra of the QPSU, QPSU/2.5% *f*-MWCNT and QPSU/5% *f*-MWCNT are presented

in Figure 3. The characteristic absorption peak of N-CH_2 at 1475 cm^{-1} in Figure 3 (a), and the sharp absorption bands at 1397 , 1364 and 1320 cm^{-1} were due to the introduction of the quaternary ammonium group^[30]. The results depict that the quaternary ammonium groups were indeed attached to the polymer, whereas in the composites, the change in the intensity ratio of the quaternary ammonium peaks was observed between the bare polymer and the composites. This may be due to the discrepancy in the polymer structures on the surface of the carbon nanotubes. Also, the intensity of the peak was broadened, as evidenced by the reduction in the relative strength of the IR signals at 1600 cm^{-1} and 750 cm^{-1} .

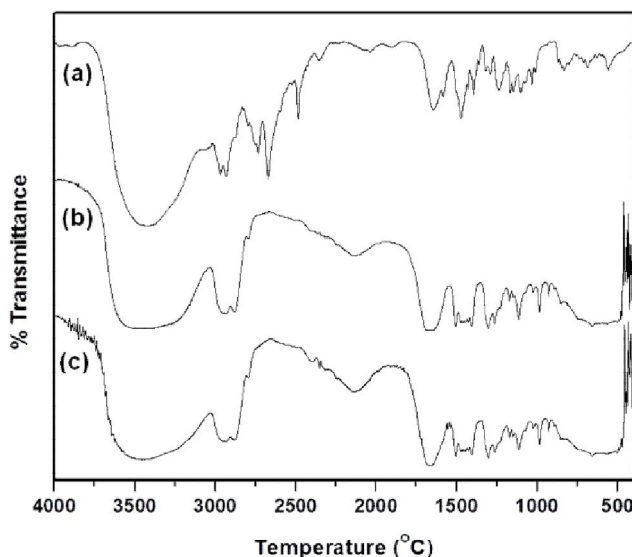


Figure 3 : FTIR spectra of (a) QPSU, (b) QPSU/2.5% *f*-MWCNT and (c) QPSU/5% *f*-MWCNT.

UV-visible spectroscopy

To elucidate the interactions between the *f*-MWCNTs and the quaternized polymer matrix, the UV-visible spectra of the QPSU and QPSU/*f*-MWCNT dispersion in dimethylformamide solvent were measured (Figure 4). The UV-Visible spectroscopy was successfully used for the quantitative characterization of the colloidal stability of the *f*-MWCNT dispersions^[37] and for the examination of the dispersion behavior which have correlations with the solubility parameters based on the interactions between the filler and the polymer^[38]. By comparing the relative height of the peak at 260 nm, we can infer that the band at 260 nm in the nanocomposite revealed a higher absorption than that

in the virgin polymer, which indicates that there is an interaction between the *f*-MWCNT and the QPSU primarily via the π - π bonding^[39,40].

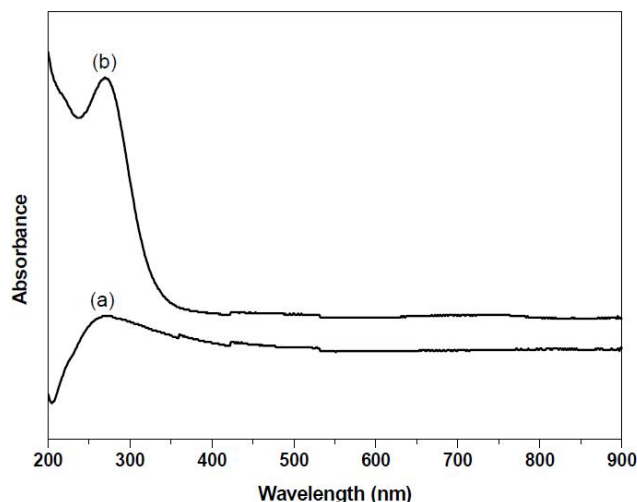


Figure 4 : UV-Visible spectra of (a) QPSU and (b) QPSU/5% *f*-MWCNT.

TGA

The effect of the *f*-MWCNTs' presence on the thermal stability of the QPSU composites was studied by means of the TGA under N_2 atmosphere, as shown in Figure 5. Figure 5(a) represents the thermogravimetric curve of the QPSU membrane. Figure 5 (b) and (c) represent the pristine MWCNT and 5% *f*-MWCNT composite respectively. Once the *f*-MWCNT was added to the polymer matrix, the thermal stability of the composite membranes was synergistically enhanced upto $550\text{ }^\circ\text{C}$, and also the 5% *f*-MWCNT possessed a higher amount of char residue (32%) than the QPSU (5%), indicating the higher thermal stability. These results illustrate that the prepared composite membranes QPSU/5% *f*-MWCNT are thermally stable at about $550\text{ }^\circ\text{C}$, which is good enough for the usage in AMFC and DMAMFCs. Considering these requirements for practical application in DMAMFCs, the composite membranes prepared using the *f*-MWCNT filler are a good choice, because they have a good ionic conductivity, low methanol permeability, good swelling resistance and good thermal stability.

XRD

In order to confirm the influence of the carbon nanotubes on the crystal structure of the QPSU, the XRD spectra of MWCNTs, bare polymer (QPSU),

Full Paper

and nanocomposites of 2.5% *f*-MWCNTs and 5% *f*-MWCNTs were studied (Figure 6). The diffraction pattern of the MWCNTs is characterized by a strong peak at $2\theta = 25.9^\circ$ ascribed to the graphite-like structure. The bare polymer show broad peak at $2\theta = 19-20^\circ$ represents the crystalline nature of the polymer. The addition of the *f*-MWCNTs into the polymer matrix did not cause a discernible change in the lattice structure of the QPSU which are shown in Figure 6. It can be seen only a small reduction in the sharpness of the crystalline peaks, as the MWCNTs were present in the polymer matrix, and a slight change in the crystalline nature of the bare polymer, i.e. its low crystallinity. The low crystallinity reveals that a more amorphous phase exists in the composite membrane, indicating that the structure of the membrane is more disordered, and the QPSU and MWCNTs are mixed uniformly. The good mixing of the QPSU and *f*-MWCNTs is useful for the enhancement of ionic conductivity^[41].

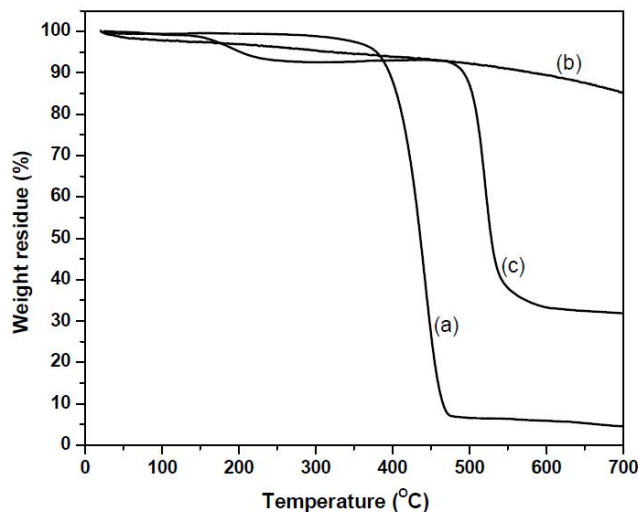


Figure 5 : TGA curves of (a) QPSU, (b) *f*-MWCNT and (c) QPSU/5% *f*-MWCNT.

TABLE 3 : Percentage of crystallinity values of prepared membranes.

Membrane	% of crystallinity
QPSU	0.76
QPSU/2.5% MWCNT	0.53
QPSU/5% MWCNT	0.37

The calculated percentage of the crystallinity of the QPSU and QPSU/*f*-MWCNT composites is given in TABLE 3. From the table, it can be seen that the percentage crystallinity of the composite in the 5 wt % of

f-MWCNT is low (0.37%). For alkaline membrane fuel cell applications, the membrane should possess amorphous behavior; in other words, low crystallinity, reveals good ionic conductivity. Hence poor crystallinity gives better performance in a fuel cell.

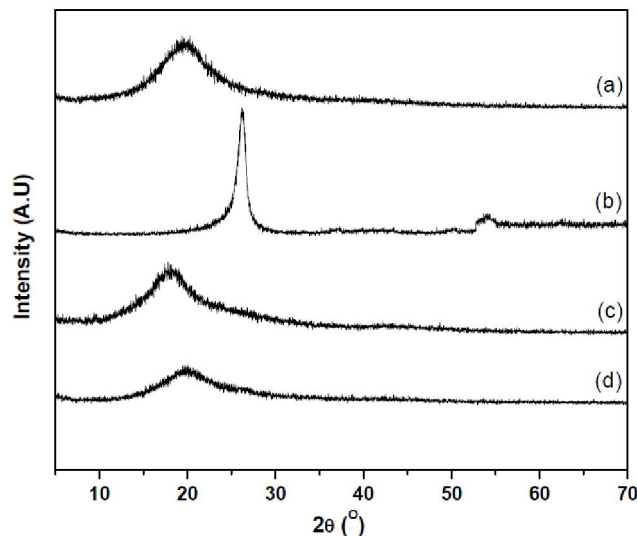


Figure 6 : XRD patterns of (a) QPSU, (b) MWCNT, (c) QPSU/2.5% *f*-MWCNT and (d) QPSU/5% *f*-MWCNT.

Mechanical properties

The extraordinary mechanical properties and large aspect ratio make the MWCNTs excellent candidates for the development of MWCNT-reinforced polymer nanocomposites. The incorporation of the MWCNTs into the QPSU can dramatically increase the tensile strength. The tensile strength of 51 MPa for the QPSU/5% *f*-MWCNT and 39 MPa for the QPSU/2.5% *f*-MWCNT, are 188% and 144% higher than that of the virgin QPSU membrane (27 MPa). The hydrophilic functional groups (-COOH) on the MWCNT were helpful in improving the interaction with the quaternized groups in the QPSU. Therefore, the strong interaction between the *f*-MWCNTs and the quaternized polymer matrix greatly enhanced the dispersion as well as the interfacial adhesion, thus strengthening the overall mechanical performance of the composite.

SEM

The surface morphology of the composite membrane was investigated by scanning electron microscopy. Figure 7 shows the SEM images of the 5% *f*-MWCNT reinforced QPSU. The *f*-MWCNTs were found to be dispersed uniformly in the quaternized poly-

mer matrix. A few white dots in the images representing the area of the *f*-MWCNTs/QPSU membrane, and this shows that the multiwalled carbon nanotubes can be effectively dispersed, when DMF was added via the described solvent evaporation method with the *f*-MWCNTs. The improved dispersion of the fine MWCNTs in the QPSU may be due to its hydrophilicity and small size, resulting in a perfect skin being formed on the surface of membrane.

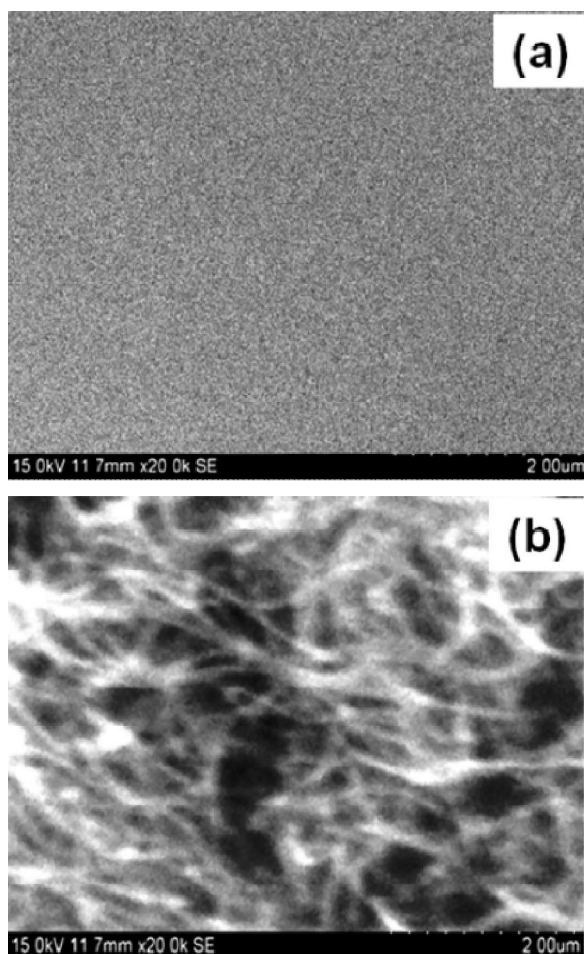


Figure 7 : SEM images of a) QPSU and b) QPSU/5% *f*-MWCNT.

Raman spectroscopy

Figure 8 represents the Raman spectrum of QPSU/5% *f*-MWCNT. The sample (5 wt % *f*-MWCNT on QPSU) exhibited two distinct bands appearing at around 1350 (D-band) and 1625 (G-band) cm^{-1} . The D-band and G-band reflect the structure of sp^3 and sp^2 hybridized carbon atoms, indicating disordered graphite, and the order state on the QPSU surfaces, respectively^[42]. Therefore, the degree of the graphitization of the QPSU/

f-MWCNT can be quantified by the intensity of the ratio of the D to G bands. The peak intensity ratios (I_D/I_G) are 0.73 for the 5% *f*-MWCNT/QPSU. There are no additional peaks present in the composite membrane, i.e. corresponding to the QPSU polymer. It clearly revealed that there is a strong interaction between the quaternized polymer and the *f*-MWCNTs.

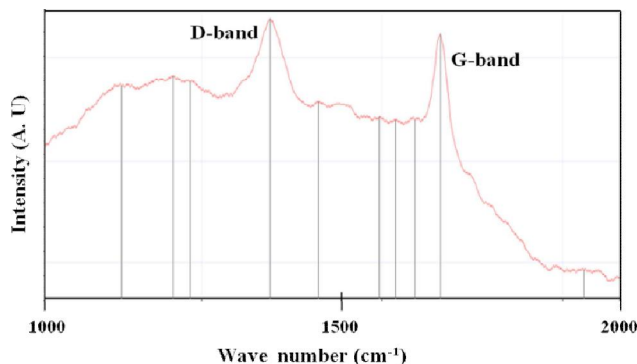


Figure 8 : Raman spectrum of QPSU/5% *f*-MWCNT.

Cyclic voltammetry studies

To test the electrocatalytic behavior of the QPSU and QPSU/*f*-MWCNT in a direct methanol alkaline membrane fuel cell (DMAMFC), cyclic voltammograms at the bare GCE, QPSU/GCE and QPSU/5% *f*-MWCNT/GCE were recorded in the presence of 0.5 M KOH and 1 M methanol with a potential range of -1.0 to +1.0 V (Vs. SCE) at a scan rate of 50 mVs^{-1} , and the results are presented in Figure 9. As shown in Figure 9, at bare GCE (a) and QPSU/GCE (b) no electrooxidation or reduction occurred. However, the QPSU/5% *f*-MWCNT/GCE (c) in the 0.5 M KOH solution exhibited a voltammogram with an increasing current, when compared to the bare GCE and QPSU/GCE. Furthermore, when the same modified electrode was kept in a mixture of 0.5 M KOH and 1 M methanol solution, a dramatic change was observed in the CVs. A large anodic peak was observed at -0.2 V, and the peak shifted slightly from the original peak (0.9 V). The increment of the catalytic current and the decrease of the overpotential are the two important factors in evaluating the catalytic effect, which proved that the as-synthesized QPSU/5% *f*-MWCNT/GCE can be effectively used in DMAFC applications too. This increase in the catalytic activity is due to the interaction between the quaternized polymer and the *f*-MWCNTs.

Full Paper

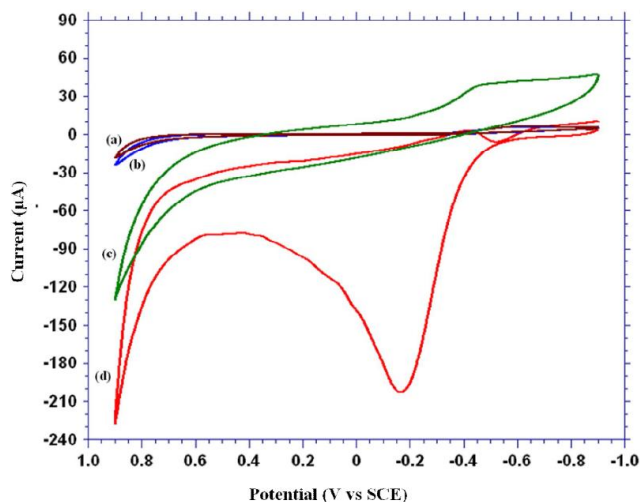


Figure 9 : Comparative cyclic voltammograms of a) bare GCE, b) QPSU, c) QPSU/5% *f*-MWCNT in 0.5M KOH and d) QPSU/5% *f*-MWCNT in 0.5M KOH + 1M methanol solution with sweep rate of 50 mVs⁻¹.

AMFC performance study

The polarization and power density curves of the QPSU, QPSU/2.5% *f*-MWCNT and QPSU/5% *f*-MWCNT, obtained from the alkaline membrane fuel cell, using Pt as the anode and Ag as the cathode catalysts, are presented in Figure 10. The measurements were taken by feeding hydrogen and oxygen with a flow rate of 20 and 40 mL/min respectively at 60 °C with a relative humidity of 77%. The alkaline membrane fuel cell with a QPSU/5% *f*-MWCNT gave a better performance than that with the QPSU/2.5% *f*-MWCNT composite and QPSU. The OCV for the QPSU/5% *f*-MWCNT was found to be 0.75 at 60 °C. In terms of power density, the QPSU/5% *f*-MWCNT shows a maximum power density of 190 mW/cm². On the whole, in terms of OCV and maximum power density, the QPSU/5% *f*-MWCNT showed better results, when compared to the QPSU/2.5% *f*-MWCNT and QPSU anion exchange membrane.

DMAMFC performance study

The performance of the QPSU/*f*-MWCNT was investigated using Pt-Ru/C and Pt/C as the anode and cathode catalysts respectively; which are depicted in Figure 11. The I-V curves showed the improved performance of the composite membranes, when compared to the virgin QPSU membrane, when DMAMFC was operated at 60 °C. The OCV of the QPSU/5% *f*-MWCNT was found to be 0.62 V and the maximum

power density of 65 mW/cm² was achieved, at a current density of 250 mA/cm².

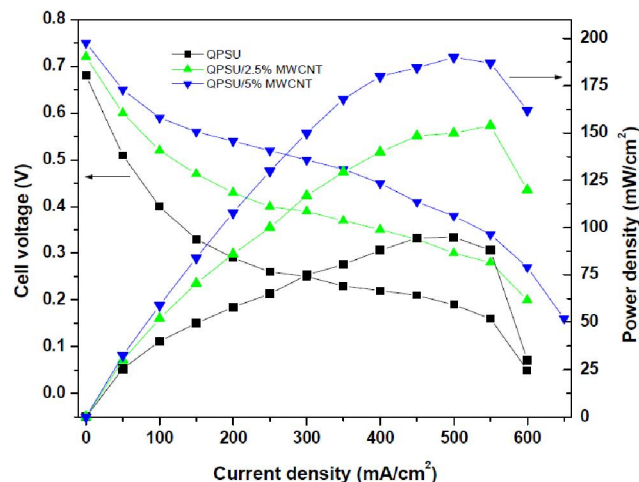


Figure 10 : AMFC performance of QPSU, QPSU/2.5% *f*-MWCNT and QPSU/5% *f*-MWCNT composite membranes.

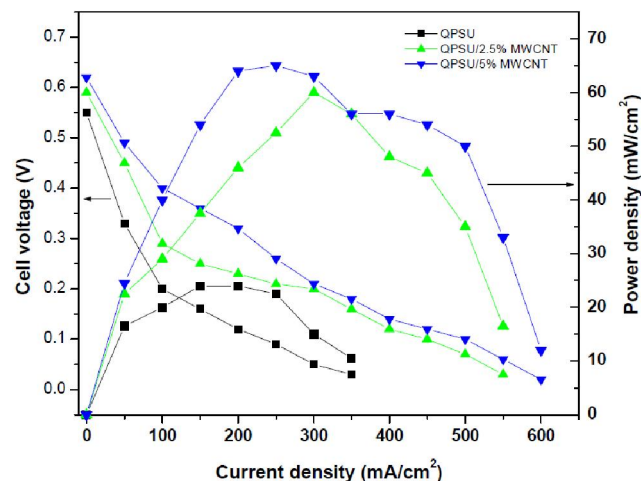


Figure 11 : DMAMFC performance of QPSU, QPSU/2.5% *f*-MWCNT and QPSU/5% *f*-MWCNT composite membranes.

CONCLUSIONS

The filler, MWCNT was functionalized by the conventional acid treatment. The composite polymer membranes based on the QPSU and *f*-MWCNT were prepared by the solution casting method. Laboratory studies like water absorption, IEC and conductivity values showed that the composite membranes possessed properties, which are suitable for work in a fuel cell environment. The thermogravimetric analysis suggested that the thermal stability of the composite membrane was adequate. The SEM results revealed that *f*-MWCNTs were distributed homogeneously throughout the poly-

mer matrix. The XRD pattern illustrated that the crystallinity of the membrane decreased with an increase in the MWCNT content; this amorphous nature could facilitate the ionic conductivity of the composite membrane. In-house alkaline membrane fuel cell comprising of the QPSU/*f*-MWCNT composite membrane was assembled and examined. The QPSU/5% *f*-MWCNT was found to show the maximum power density (190 mW cm⁻²) and open circuit voltage (0.75 V). The composite membranes were also subjected to cyclic voltammetry studies for methanol oxidation and the obtained results showed that the prepared composite membranes which could also be applied in direct methanol alkaline membrane fuel cell.

ACKNOWLEDGEMENT

Financial support from the Department of Science and Technology (DST), New Delhi, India (Letter No. SR/S2/CMP-06/2008, dated 21-08-2008) is gratefully acknowledged. DST-FIST and UGC-DRS, Department of Chemistry, Anna University providing the instrument facility is gratefully acknowledged.

REFERENCES

- [1] H.A.Gasteiger, S.S.Kocha, B.Sompalli, F.T.Wagner; Applied Catalysis B: Environmental, **56**, 9-35 (2005).
- [2] L.Carrette, K.A.Friedrich, U.Stimming; Chemical Physics and Physical Chemistry, **1**, 5 – 39 (2001).
- [3] R.Borup, J.Meyers, B.Pivovar; Chemical Review **107**, 3904–3951 (2007).
- [4] G.F.Mc Lean, T.Niet, S.Prince-Richard, N.Djilali; International Journal of Hydrogen Energy, **27**, 507–526 (2002).
- [5] J.R.Varcoe, R.C.T.Slade; Fuel Cells, **5**, 187–200 (2005).
- [6] P.K.Shen, C.W.Xu, H.Meng, R.Zeng; Anion exchange membrane fuel cells. In: X.W. Zhang (Ed); Advances in fuel cells. Kerala, India: Research Signpost; 149–179 (2005).
- [7] J.S.Spendelow, A.Wieckowski; Physical Chemistry Chemical Physics, **9**, 2654–2675 (2007).
- [8] M.Cifrain, K.V.Kordesch; Journal of Power Sources, **127**, 234–242 (2004).
- [9] E.Gulzow, M.Schulze; Journal of Power Sources **127**, 243–251 (2004).
- [10] J.R.Varcoe, R.C.T.Slade, H.Y.E.Lam; Chemical Communication, **1428**, 1429 (2006).
- [11] R.Dillon, S.Srinivasan, A.S.Arco, V.Antonucci; Journal of Power Sources, **127**, 112–126 (2004).
- [12] Y.Wan, K.A.M.Creber, B.Peppley, V.T.Bui; Journal of Membrane Science, **284**, 331-338 (2006).
- [13] J.Fang, P.K.Shen; Journal of Membrane Science, **285**, 317-322 (2006).
- [14] L.Li, J.Wang; Journal of Membrane Science, **262**, 1-4 (2005).
- [15] F.Yi, X.Yang, Y.Li; Polymers for Advanced Technologies, **10**, 473-475 (1999).
- [16] R.C.T.Slade, J.R.Varcoe; Solid State Ionics, **176**, 585-597 (2005).
- [17] J.J.Kang, W.Y.Li, Y.Lin, X.Li, X.R.Xiao, S.B.Fang; Polymers for Advanced Technologies, **15**, 61-64 (2004).
- [18] R.Vinodh, K.A.Bhat, D.Sangeetha; Journal of Polymer Research, **18**, 1469–1477 (2011).
- [19] F.Zhang, H.Zhang, C.Qu; Journal of Materials Chemistry, **21**, 12744-12752 (2011).
- [20] A.Pud, N.Ogurtsov, A.Korzhenko, G.Shapoval; Progress in Polymer Science, **28**, 1701-1703 (2003).
- [21] R.Gangopadhyay, A.De; Chemistry of Materials, **12**, 608-622 (2000).
- [22] J.Gao, M.E.Itkis, A.Yu, E.Bekyarova, B.Zhao, R.C.Haddon; Journal of American Chemical Society, **127**, 3847-3454 (2005).
- [23] M.Moniruzzaman, K.I.Winey; Macromolecules, **39**, 5194-5195 (2006).
- [24] S.H.Joo, C.Pak, E.A.Kim, Y.H.Lee, H.Chang, D.Seung, Y.S.Choi, J.B.Park, T.K.Kim; Journal of Power Sources, **180**, 63-70 (2008).
- [25] R.Vinodh, D.Sangeetha; Journal of Material Science, **47**, 852–859 (2012).
- [26] T.Xu, W.Yang; Journal of Membrane Science, **190**, 159–166 (2001).
- [27] G.J.Hwang, H.Ohya; Journal of Membrane Science, **140**, 195–203 (1998).
- [28] F.C.Ding, S.J.Wang, M.Xiao, Y.Z.Meng; Journal of Power Sources, **164**, 488-495 (2007).
- [29] Y.F.Lin, C.Y.Yen, C.C.M.Ma, S.M.Liao, C.H.Hung, Y.H.Hsiao; Journal of Power Sources, **165**, 692-700 (2007).
- [30] R.Vinodh, M.Purushothaman, D.Sangeetha; International Journal of Hydrogen Energy, **36**, 7291-7302 (2011).
- [31] D.M.Delozier, K.A.Watson, J.G.Smith Jr., T.C.Clancy, J.W.Connell; Macromolecules, **39**, 1731-1739 (2006).

Full Paper

- [32] D.H.Xu, Z.G.Wang; *Macromolecules*, **41**, 815-825 (2008).
- [33] A.A.Koval'chuk, V.G.Shevchenko, A.N.Shchegolikhin, P.M.Nedorezova, A.N.Klyamkina, A.M.Aladyshev; *Macromolecules*, **41**, 7536-7542 (2008).
- [34] D.McIntosh, V.N.Khabashesku, E.V.Barrera; *Journal of Physical Chemistry C*, **111**, 1592-600 (2007).
- [35] E.Bekyarova, M.E.Itkis, N.Cabrera, B.Zhao, A.P.Yu, J.B.Gao, R.C.Haddon; *Journal of American Chemical Society*, **127**, 5990-5995 (2005).
- [36] R.A.Hatton, A.J.Miller, S.R.P.Silva; *Journal of Materials Chemistry*, **18**, 1183-1192 (2008).
- [37] L.Jiang, L.Gao, J.Sun; *Journal of Colloid and Interface Science*, **260**, 89-94 (2003).
- [38] H.T.Ham, Y.S.Choi, I.J.Chung; *Journal of Colloid and Interface Science*, **286**, 216-223 (2005).
- [39] D.Baskaran, J.W.Mays, M.S.Bratcher; *Chemistry of Materials*, **17**, 3389-3397 (2005).
- [40] F.Frehill, M.Panhuis, N.A.Young, W.Henry, J.Hjelm, J.G.Vos; *Journal of Physical Chemistry B*, **109**, 13205-13209 (2005).
- [41] E.D.Wang, T.S.Zhao, W.W.Yang; *International Journal of Hydrogen Energy*, **35**, 2183-2189 (2010).
- [42] N.Yao, V.Lordi, S.X.Ma, E.Dujardin, A.Krishnan, M.M.Treacy, T.W.Ebbesen; *Journal of Materials Research*, **13**, 2432-2437 (1998).